Solid State Communications 275 (2018) 48–52

Contents lists available at ScienceDirect

Solid State Communications

journal homepage: www.elsevier.com/locate/ssc

Communication

Effect of magnetic field on the flux pinning mechanisms in Al and SiC co-doped MgB_2 superconductor

N.S. Kia [a], S.R. Ghorbani [a,*], H. Arabi [a], M.S.A. Hossain [b]

[a] Renewable Energies, Magnetism and Nanotechnology Lab, Department of Physics, Faculty of Science, Ferdowsi University of Mashhad, Mashhad, Iran
[b] Institute for Superconducting and Electronic Materials, Australian Institute for Innovative Materials, University of Wollongong, Faculty of Engineering, North Wollongong, NSW 2519, Australia

ARTICLE INFO

Communicated by F. Peeters

Keywords:
MgB_2 superconductor
Critical current
Flux pinning
Single vortex-pinning

ABSTRACT

MgB_2 superconductor samples co-doped with 0.02 wt. Al_2O_3 and 0–0.05 wt. SiC were studied by magnetization – magnetic field (M-H) loop measurements at different temperatures. The critical current density has been calculated by the Bean model, and the irreversibility field, H_{irr}, has been obtained by the Kramer method. The pinning mechanism of the co-doped sample with 2% Al and 5% SiC was investigated in particular due to its having the highest H_{irr}. The normalized volume pinning force $f = F/F_{max}$ as a function of reduced magnetic field $h = H/H_{irr}$ has been obtained, and the pinning mechanism was studied by the Dew-Houghes model. It was found that the normal point pinning (*NPP*), the normal surface pinning (*NSP*), and the normal volume pinning (*NVP*) mechanisms play the main roles. The magnetic field and temperature dependence of contributions of the *NPP, NSP*, and *NVP* pinning mechanisms were obtained. The results show that the contributions of the pinning mechanisms depend on the temperature and magnetic field. From the temperature dependence of the critical current density within the collective pinning theory, it was found that both the δl pinning due to spatial fluctuations of the charge-carrier mean free path and the δT_c pinning due to randomly distributed spatial variations in the transition temperature coexist at zero magnetic field in co-doped samples. Yet, the charge-carrier mean-free-path fluctuation pinning (δl) is the only important pinning mechanism at non-zero magnetic fields.

1. Introduction

Superconductivity was discovered in 1911 as an obscure phenomenon. Afterwards, a large number of research discoveries occurred in relation to this concept. In 2001, the MgB_2 compound was found to be a metallic and easily produced superconductor [1]. This new superconductor compound received a great deal of interest due to its specific features. MgB_2 is, the like low temperature superconductors (LTS), highly isotropic, which is caused by its large coherence length, but unlike the LTS, it has the high critical temperature of $T_c = 39$ K MgB_2 compound lacks sufficient flux pinning centers for high performance, however, due to the weak connections between the grains in the structure [2]. That is why MgB_2 has low critical current density, J_c. Many parameters, e.g., the irreversibility field, H_{irr}, the upper critical field, H_{c2}, the flux pinning, and the connectivity, control the J_c. Therefore, improvement of the J_c properties in MgB_2 has been mostly aimed at enhancing the H_{irr}, the flux pinning capability, and H_{c2} by ion irradiation or chemical doping [2–8]. Chemical doping has been proved to be a simple and effective way to introduce pinning centers into MgB_2 superconductor or to improve the upper critical field. It was found that carbon containing dopants [9–13] and silicon compounds [9,14,15] are especially effective for improving the J_c properties of MgB_2 in high magnetic fields. It was also found that Al_2O_3 nano-particles create pinning centers throughout the structure by Al substitution for Mg. Up to 5 wt% of this Al-oxide has been shown to improve the critical current density J_c and irreversibility field H_{irr} [3].

The pinning mechanism control the current-density decay behavior. Numerous investigations have been performed with the purpose of understanding vortex-pinning mechanisms [7,8,16–19]. In a multiband superconductor, it was found that different field dependence of the gaps play an important role in defining its vortex dynamics [16]. Kwok et al. [18] studied vortex pinning mechanism through an emerging novel synergistic approach that combined theory, experiments and large-scale simulations of vortex matter in mixed-pinning landscapes. They found a quantitative correlation between the observed critical current density and multi-scale mixed pinning landscapes by using large-scale time dependent Ginzburg–Landau approach.

* Corresponding author.
E-mail address: sh.ghorbani@um.ac.ir (S.R. Ghorbani).

https://doi.org/10.1016/j.ssc.2018.03.013
Received 7 December 2017; Received in revised form 17 March 2018; Accepted 20 March 2018
Available online 21 March 2018

There are two main kinds of formalism for investigating pinning mechanisms. The first is based on pinning center geometries and their dimensions, such as point centers (zero-dimensional, 0D), surface pinning centers (two-dimensional, 2D), and volume pinning centers (three-dimensional, 3D). Flux pinning mechanisms based on these kinds of pinning centers are scaled by the theories of Dew-Hughes [8] and Kramer [7]. Studies of the pinning mechanisms in terms of this model indicate that a variety of pinning mechanisms, e.g. normal point pinning, normal surface pinning, and normal volume pinning mechanisms, exist in nano-Si and $SiCl_4$ doped MgB_2 [20] and in $Fe_{1.06}Te_{0.6}Se_{0.4}$ single crystal [21].

The second kind of formalisms relates to the basic pinning mechanisms, which correspond to the randomly distributed spatial variations in the transition temperature T_c, which is called δT_c, and the spatial fluctuation of the charge-carrier mean free path, the so-called δl, which is mostly due to crystal lattice defects, in type-II superconductors [22,23]. It was found that the δT_c pinning is the main flux pinning mechanism in bulk cuprate [24] and pure MgB_2 bulk and thin films [25–27]. It has been reported, however, that δl pinning is the most important effect in thin films of Y-based high-T_c superconductors [23]. It was also reported that both mechanisms coexist in nanoparticle doped-MgB_2 [15,28] and Fe-based superconductor samples [29], depending on the temperature and magnetic field.

The current-density decay behavior is governed by the pinning mechanism. Due to the defect and nanoparticle-inclusion-related J_c-field enhancement in chemically co-doped MgB_2, the pinning mechanisms are of interest in such samples from the points of view of both the fundamental physics and of applications. There are some co-doping reports on MgB_2, as well. As found in Ref. [5], Al_2O_3 and SiC co-doping of MgB_2 compound, $Mg_{1-x}Al_x(B_{1-y}C_y)_2$ with $x = 2\%$ and $y = 1\%$, is more effective than sole Al-doping for improvement of the critical current density J_c. Nevertheless, the flux pinning mechanism for Al_2O_3 and SiC co-doped MgB_2 has not been studied systematically so far.

In this paper, the flux pinning mechanisms for Al_2O_3 and SiC co-doped MgB_2 are discussed in the framework of both the Dew-Hughes model and the collective theory. It was found that a variety of pinning mechanisms, e.g. normal point pinning, normal surface pinning, and normal volume pinning mechanisms, exist in co-doped MgB_2 samples. The results show that both the δl and δT_c pinning mechanisms co-exist at zero magnetic field in the Al_2O_3 and SiC doped MgB_2 samples. At non-zero magnetic field, the charge-carrier mean-free-path fluctuation pinning (δl) is the only important pinning mechanism.

2. Experimental procedure

Stoichiometric superconducting compounds of $Mg_{1-x}Al_x(B_{1-y}C_y)_2$ with $x = 2\%$ and $y = 0$–5% has been prepared by the solid state method, which been reported thoroughly elsewhere [6]. Microstructures, lattice parameters, magnetization and normal state resistivity were characterized by using a field emission gun-scanning electron microscope (FEG--SEM), X-ray diffractometer (XRD) [6]. X-ray diffraction results revealed that all the samples were crystallized in the MgB_2 structure as the major phase, although a few impurity lines of MgO and Mg_2Si were observed in all the samples. The microstructures studies by the FEG-SEM show that the grain size seems to be smaller, more compacted and homogeneous for the co-doped sample compared to un-doped and mono-doped samples [6]. It was also found [6] that the critical temperature declined from 37.38 K to 34.25 K with increasing co-doping concentration and the electrical resistivity at $T = 40$ K, ρ (40 K), increased from 28 μΩ cm to 122 μΩ cm for pure sample and the sample with the highest doping concentration of 2% Al_2O_3 and 5% SiC, respectively. Although, the lattice parameters did not shift critically. But comparatively, the lattice parameter with a-axis direction decreased faster than the c-axis one with increasing addition of SiC. It could be easily revealed that C is substitute on B sites in the ab-plane. However, the c-axis lattice parameter was almost unchanged and only slightly altered when the percent of Al2O3 increased. The magnetic hysteresis loops were measured using a physical properties measurement system (PPMS, Quantum Design). The critical current density was calculated by using the Bean approximation.

3. Results and discussions

The critical current density J_c as a function of magnetic field at the temperature of $T = 10$ K is shown in Fig. 1 for all samples, including pure (undoped) and co-doped samples with different doping percentages. As is illustrated in Fig. 1, co-doping with 2% Al_2O_3 and 0–5% SiC, improved the J_c of MgB_2 at high magnetic field. Among them, however, the 1 wt% SiC doping was more effective for enhancement of J_c. The J_c decreased in higher fields, however, so that, in the magnetic field of 4.2 T, it is equal to the value for an SiC-doped sample with 3% wt, and for higher than that field, it is reduced even more. In magnetic fields of more than 1.5 T, the negative slope of $J_c(H)$ is almost the same for the three samples that were SiC-doped with 3%, 4% and 5% wt. At magnetic fields smaller than 2 T, the J_c after co-doping with 2% Al_2O_3 and both 2 and 5% SiC is smaller than that of the undoped sample.

The irreversibility field H_{irr} was obtained by the Kramer method [7] from the linear intercept of the curve of $J_c^{0.5}B^{0.25}$ vs. magnetic field B, as shown in the inset of Fig. 2. The obtained irreversibility fields H_{irr} are shown in Fig. 2 for the undoped and all the doped samples.

As can be seen in Fig. 2, the pure (undoped) MgB_2 sample has the lowest irreversibility field, and the co-doping with 2% Al_2O_3 and 0–5% SiC enhances the H_{irr} at all temperatures. At lower temperature, the co-doping is more effective for the irreversibility field. In addition, results show that the sample with 2 wt% Al_2O_3 and 5 wt% SiC-doping has the highest irreversibility field at all temperatures. So, the flux pinning mechanism for this sample, which show the most improvement in H_{irr} as a result of improved flux pinning centers, has been investigated.

To investigate the flux pinning mechanisms, the co-doped sample with 2 wt% Al and 5 wt% was studied by the Dew-Hughes method [8]. According to this model, the flux pinning mechanism in superconducting materials is defined by the following relation:

$$f_p = Ah^p(1-h)^q \tag{1}$$

Where $f_p = F_p/F_{p,max}$ is normalized volume pinning force, $F_p = |J_c \times \mu_0 H|$, and h is the ratio of the magnetic field to the irreversibility field, H/H_{irr}. The f_p has its maximum at $h_{max} = p/p+q$. Therefore, A is a normalization coefficient with the value of $(h_{max}^p(1-h_{max})^q)^{-1}$, and then:

$$f_p = \frac{h^p(1-h)^q}{h_{max}^p(1-h_{max})^q} \tag{2}$$

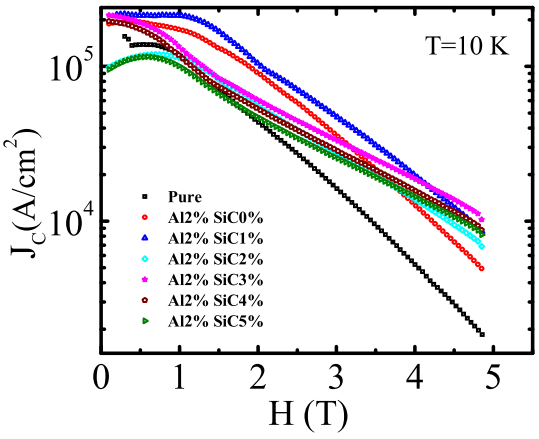

Fig. 1. Logarithmic changes of the in-field critical current density in response to different magnetic fields at a certain temperature $T = 10$ K for samples that were Al-doped with 2 wt% and SiC-doped with 0–5 wt%, with an undoped sample shown for reference.

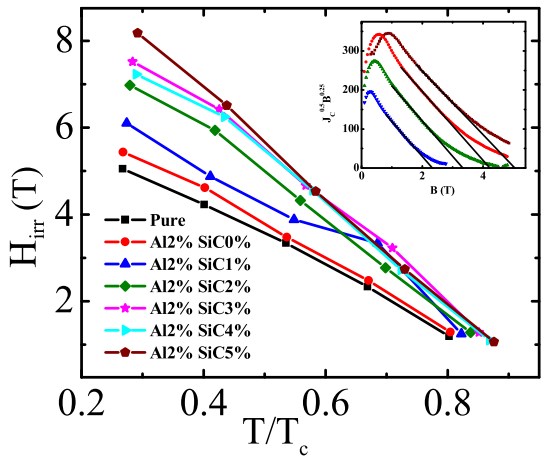

Fig. 2. Irreversibility field vs. reduced temperature for co-doped and undoped samples. Inset: Kramer method for obtaining H_{irr}.

where p and q are parameters which determine the flux pinning mechanism. In this model $p=1$ and $q=2$ describe normal point pinning (*NPP*), $p=1/2$ and $q=2$ describe normal surface pinning (*NSP*), and $p=0$ and $q=2$ describe normal volume pinning (*NVP*) mechanisms, which play the main roles in flux pinning in the superconductor materials.

Fig. 3 shows the results of *f-h* for the Al_2O_3 2% and SiC 5% co-doped MgB_2 sample at different temperatures. The three main pinning mechanisms have been added to Fig. 3 as solid curves.

It is obvious from Fig. 3 that the experimental data are located between the two master curves of the *NPP* and the *NSP* mechanisms for h h_{max}, while for $h > h_{max}$, the data reside between the *NSP* and the *NVP* curves. The contributions have been calculated as:

$$f_{P.T} = a_{NPP}f_{NPP} + a_{NSP}f_{NSP} + a_{NVP}f_{NVP} \tag{3}$$

where a_{NPP}, a_{NSP}, and a_{NVP} are fitting parameters, which represent the normal point pinning, the normal surface pinning, and the normal volume pinning effects, respectively, with

$$a_{NPP} + a_{NSP} + a_{NVP} = 1. \tag{4}$$

In this case, the best fitting includes the contributions from normal point pinning a_{NPP}, normal surface pinning a_{NSP}, and normal volume pinning a_{NVP}.

Fig. 4 shows the contribution of each mechanism separately in

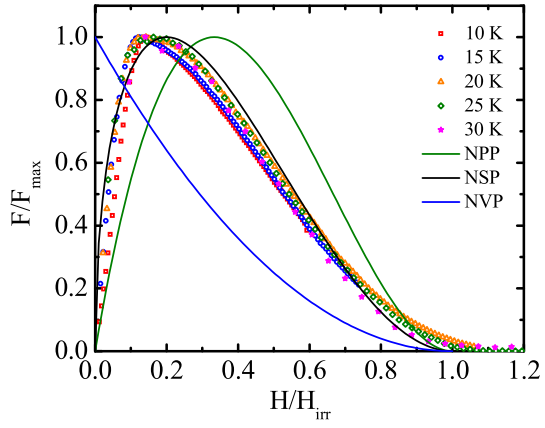

Fig. 3. Normalized pinning force vs. H/H_{irr} at different temperatures for Al_2O_3 2% and SiC 5% co-doped sample, with three flux pinning models based on the Dew-Hughes theory shown by solid curves.

different magnetic fields and at different temperatures. It is found that the pinning mechanism contributions depend on the magnetic field. The normal surface pinning mechanism originates from grain boundaries, and that is why it is the only mechanism which exists in field regions of both $h < h_{max}$ and $h > h_{max}$ at all temperatures. For $h < h_{max}$ there is just the normal point pinning mechanism that contributes with the *NSP* mechanism. This mechanism is due to dopants, and therefore, in lower fields, it could have a main role in flux pinning in the form of good pinning centers, although the contribution of the *NSP* mechanism increases with increasing magnetic field, so that near the reduced field of $h = h_{max}$, it is the mechanism that plays the main role in the flux pinning at all temperatures. In a reduced field of $h > h_{max}$, the *NPP* mechanism does not contribute to the pinning force. In this region, both the normal volume pinning *NVP* and the surface pinning mechanism *NSP* coexist, and their contributions depend on temperature. The results clearly show that the surface pinning becomes dominant at all temperatures. The normal volume pinning is due to impurities. With increasing magnetic field, more flux vortices penetrate into the sample, and the inter-flux-vortex spacing, a, becomes shorter compared to the dimensions of the MgO and Mg_2Si impurities, which had acted as normal volume pinning centers. Microstructure studies of $SiCl_4$-doped MgB_2 samples by transmission electron microscopy (TEM) support these results [30,31].

In Fig. 5, the temperature dependence of the pinning mechanisms has been compared for the two reduced magnetic field of $h = 0.048$ and $h = 0.451$ that are located in the $h < h_{max}$ and $h > h_{max}$ regions, respectively. In the $h < h_{max}$ region, the contributions of both the *NPP* mechanism and the *NSP* mechanism depend strongly on temperature. The *NPP* mechanism is the dominant effect at the reduced temperature of $T/T_c < 0.4$, but at higher reduced temperature, the *NSP* mechanism is more effective. In the $h > h_{max}$ region, however, both the *NSP* and the *NVP* effects weakly depend on temperature, but the *NSP* mechanism is the dominant mechanism over the whole range of reduced temperature studied here.

In order to further understand, the critical current-density results shown in Fig. 1, the real pinning mechanism was studied according to the collective theory [22]. Based on this theory, there is a crossover field, B_{sb}, that marks the transition from single vortex behavior to small vortex bundle behavior in the magnetic field dependence of the critical current density. At fields smaller than the B_{sb}, the critical current density would not depend on magnetic field and the single vortex-pinning mechanism governs the vortex lattice, $B_{sb} \propto J_{sv}H_{c2}$, where J_{sv} is the critical current density in the single vortex pinning regime. At fields larger than the crossover field, there is a new regime which is named the small bundle-pinning regime, where the critical current density decreases exponentially with magnetic field as:

$$J_c(B) \approx J_c(0)\exp\left[-(B/B_0)^{3/2}\right] \tag{5}$$

where B_0 is a normalization parameter of the order of B_{sb}, and both B_0 and $J_c(0)$ could be inferred by fitting the experimental critical current data with Eq. (5). The critical current density continues to decrease exponentially up to another crossover field, B_{lb}, which marks the transition to the large bundle-pinning regime, for $B > B_{lb}$, the critical current density decreases by a power law as $J_c(B) \propto B^{-\beta}$.

In the single vortex-pinning regime, Griessen et al. derived [23] the temperature dependences of the critical current density J_c for both the δT_c and δl pinning mechanisms, which are associated with spatial fluctuations of the transition temperature and the charge-carrier mean-free-path fluctuations, respectively. They found the following expression for the temperature dependence of the normalized critical current density for both the δT_c and δl pinning mechanisms:

$$\frac{J_c(t)}{J_c(0)} \propto (1-t^2)^{5/2}(1+t^2)^{-1/2} \tag{6}$$

for the δl pinning, and for the δT_c pinning, it is described as:

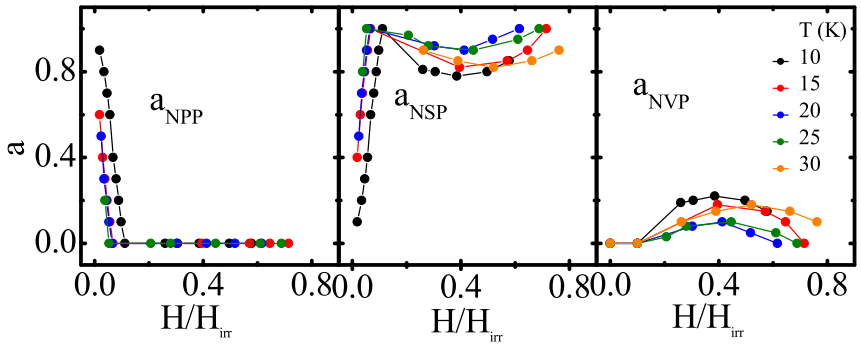

Fig. 4. Contribution of each flux pinning mechanism in different magnetic fields and at different temperatures for Al_2O_3 2% and SiC 5% co-doped MgB_2 sample.

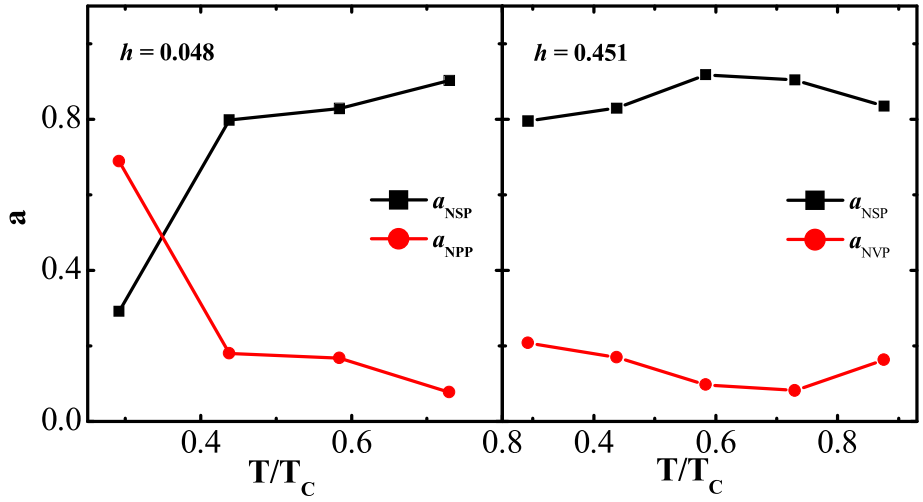

Fig. 5. The temperature dependence of the contribution of each mechanism at certain reduced magnetic fields.

$$\frac{J_c(t)}{J_c(0)} \propto (1-t^2)^{7/6}(1+t^2)^{5/6} \tag{7}$$

where $t = T/T_c$. The theoretical curves obtained, which are based on the models of both the δl and the δT_c pinning, are shown by the solid curves in Fig. 6. As shown in Fig. 6, the experimental result at zero magnetic field resides in between the two theoretical curves of the δl and the δT_c pinning mechanisms. Therefore, the δl and the δT_c pinning coexist. The T_c fluctuation in MgB_2 is due to Mg deficiency due to the formation of MgO and Mg_2Si impurity phases [6,25], which are more effective for flux pinning at the higher magnetic field as can be seen in Fig. 1. Partial dopant substitution into the lattice, which leads to a broad T_c distribution in the sample [32]. It is the inter-grain boundaries and the nanoparticle inclusions inside the MgB_2 grains results to induced point pining centers inside grains as had been reported before for the Si-doped MgB_2 by the TEM studies [33]. The point pining centers enhanced electron scattering, which is caused the mean free path fluctuations and hence the δl pinning. The mean free path, $l = v_F\,\tau = v_F/\Gamma$, [34] was calculated by considering the scattering rate of $\Gamma = \varepsilon_0\rho_0\,(\omega_{p\sigma}^2 + \omega_{p\pi}^2) = 1/\tau$, where the $\omega_{p\sigma} = 6.23$ eV and $\omega_{p\pi} = 3.40$ eV are the mean values of the plasma frequencies [35] of σ and π bands, respectively, ρ_0 is the normal state resistivity, and ε_0 is the vacuum permittivity. Using the mean value of the Fermi velocity $v_F = 5.1 \times 10^5$ ms−1 [28] and the resistivity at 40 K, the mean free path decreases from 1.8 nm for pure sample to 0.4 nm for the co-doped sample of 2% Al2O3 doping and 5% SiC doping, which is in good agreement with the observed enhancement in H_{irr} as can be seen in Fig. 2.

For the magnetic field of smaller than 1 T, the temperature dependence of the J_c is found to be in agreement with coexist of both the δl and the δT_c pinning mechanisms. However, the δl pinning mechanism

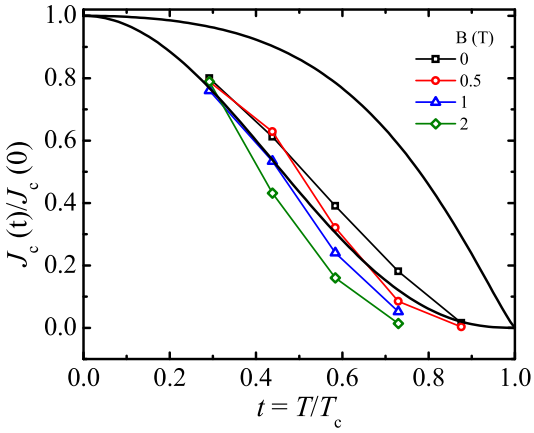

Fig. 6. Temperature dependence of the normalized critical current density at magnetic fields of 0 T, 0.5 T, 1 T, and 2 T. The solid curves represent the δT_c and δl pinning.

contribution is dominant mechanism and it is more important than δT_c mechanism at studied temperatures. As can be seen in Fig. 6, the temperature dependence of the J_c deviates from the δl pinning mechanism model for magnetic fields higher than 1 T at the reduced temperatures higher than $t = 0.4$. This indicates that the vortex pinning model may not be valid in the single vortex region for higher magnetic fields. This is because there is a small bundle-pinning regime at fields higher than the crossover field B_{sb}. In this region, it is necessary to modify the temperature dependence of the normalized critical current density for both the

δl and the δT_c pinning mechanisms in Eqs. (6) and (7), respectively.

In two-band superconductors the vortex patterns depend on the superconducting length scales (λ and ξ) associated with each band. Furthermore, disorders play an important role in pinning mechanism in doped bulk samples and therefore the superconducting length scales become highly dependent on mean free path, l. Recently, vortex structures in thin epitaxial films of the MgB_2 superconductor was investigated by scanning Hall probe microscopy (SHPM) [17]. They suggested new mechanism for spontaneous symmetry breaking in the systems of superconducting vortices at low fields. It is due to the presence of vortex repulsions with two different length scales of the two distinct superconducting bands. Therefore, it is necessary to modify the temperature dependence of the normalized critical current density for both the δl and the δT_c pinning mechanisms in Eqs. (6) and (7), respectively, at the reduced temperatures higher than $t = 0.4$. In order to further understanding of the pinning mechanism in this region, these results suggest a numerical simulations with considering different field dependence of the gaps and disorders rules in defining vortex dynamics in a bulk multiband superconductors.

In conclusion, it was found that 2 wt% Al_2O_3 and 0–5 wt% SiC co-dopants improve the critical current density at high magnetic fields, which indicates that stronger and more plentiful pinning centers are produced by these chemical co-dopants. The pinning mechanisms were studied in terms of the different pinning models, which indicates that a variety of pinning mechanisms, e.g. normal point pinning, normal surface pinning, and normal volume pinning mechanisms, coexist in co-doped MgB_2 samples. The results show that the contributions of the pinning mechanisms depend on the temperature and magnetic field. Studies of the basic pinning mechanisms in term of the collective pinning model shows that both δl pinning due to spatial fluctuations of the charge-carrier mean free path and δT_c pinning due to the randomly distributed spatial variations in the transition temperature coexist at zero magnetic field in the co-doped samples, although the charge-carrier mean-free-path fluctuation pinning (δl) is the main important pinning mechanism at non-zero magnetic fields.

Acknowledgments

The work was supported by the Ferdowsi University of Mashhad (Grant no. 3/42163).

References

[1] J. Nagamatsu, N. Nakagawa, T. Muranaka, Y. Zenitani, J. Akimitsu, Nature 410 (2001) 63.
[2] Y. Bugoslavsky, G.K. Perkins, X. Qi, L.F. Cohen, A.D. Caplin, Nature 410 (2001) 563.
[3] I.A. Ansari, M. Shahabuddin, K.A. Ziq, A.F. Salem, V.P.S. Awana, M. Husain, H. Kishan, Supercond. Sci. Technol. 20 (2007) 827.
[4] S.X. Dou, V. Braccini, S. Soltanian, R. Klie, Y. Zhu, S. Li, X.L. Wang, D. Larbalestier, Appl. Phys. Lett. 96 (2004) 7549.
[5] K. Shaikh, M. Shahabuddi, I.A. Ansari, N.S. Alzayed, Latest Res. Sci. Technol. 2 (2013) 55.
[6] S. Barua, D. Patel, N. Alzayed, M. Shahabuddin, J.M. Parakkandy, M.S. Shah, Z. Ma, M. Mustapić, M.S.A. Hossain, J.H. Kim, Mater. Lett. 139 (2014) 333.
[7] E.J. Kramer, J. Appl. Phys. 44 (1973) 1360.
[8] D. Dew-Hughes, Phil. Mag. 30 (1974) 293.
[9] S.X. Dou, S. Soltanian, J. Horvat, X.L. Wang, S.H. Zhou, M. Ionescu, H.K. Liu, P. Munroe, M. Tomsic, Appl. Phys. Lett. 81 (2002) 3419.
[10] S.X. Dou, W.K. Yeoh, J. Horvat, M. Ionescu, Appl. Phys. Lett. 83 (2003) 4996.
[11] Y.W. Ma, X.P. Zhang, G. Nishijima, K. Watanabe, S. Awaji, X.D. Bai, Appl. Phys. Lett. 88 (2006), 072502.
[12] H. Yamada, M. Hirakawa, H. Kumakura, H. Kitaguchi, Supercond. Sci. Technol. 19 (2006) 175.
[13] M.S.A. Hossain, J.H. Kim, X. Xu, X.L. Wang, M. Rindfleisch, M. Tomic, M.D. Sumption, E.W. Collings, S.X. Dou, Supercond. Sci. Technol. 20 (2007) L51.
[14] X.L. Wang, Z.X. Cheng, S.X. Dou, Appl. Phys. Lett. 90 (2007), 042501.
[15] S.R. Ghorbani, X.L. Wang, S.X. Dou, S.-I.K. Lee, M.S.A. Hossain, Phys. Rev. B 78 (2008), 184502.
[16] J. Kim, N. Haberkorn, E. Nazaretski, R. de Paula, T. Tan, X.X. Xi, T. Tajima, R. Movshovich, L. Civale, Solid State Commun. 204 (2015) 56.
[17] P.J. Curran, W.M. Desoky, M.V. Milošević, A. Chaves, J.-B. Laloë, J.S. Moodera, S.J. Bending, Sci. Rep. 5 (2015) 15569.
[18] W.-K. Kwok, U. Welp, A. Glatz, A.E. Koshelev, K.J. Kihlstrom, G.W. Crabtree, Rep. Prog. Phys. 79 (2016), 116501.
[19] J. Lombardo, Z.L. Jelic, X.D.A. Baumans, J.E. Scheerder, J.P. Nacenta, V.V. Moshchalkov, J. Van de Vondel, R.B.G. Kramer, M.V. Milosevic, A.V. Silhanek, Nanoscale 10 (2018) 1987.
[20] S.R. Ghorbani, M. Hosseinzadeh, X.L. Wang, Supercond. Sci. Technol. 28 (2015), 125006.
[21] S.J. Hossaini, S.R. Ghorbani, H. Arabi, X.L. Wang, C.T. Lin, Solid State Commun. 246 (2016) 29.
[22] G. Blatter, M.V. Feigel'man, V.B. Geshkenbein, A.I. Larkin, V.M. Vinokur, Rev. Mod. Phys. 66 (1994) 1125.
[23] R. Griessen, Hai-hu Wen, A.J.J. van Dalen, B. Dam, J. Rector, H.G. Schnack, S. Libbrecht, E. Osquiguil, Y. Bruynseraede, Phys. Rev. Lett. 72 (1994) 1910.
[24] H.H. Wen, Z.X. Zhao, Y.G. Xiao, B. Yin, J.W. Li, Physica C 251 (1995) 371.
[25] M.J. Qin, X.L. Wang, H.K. Liu, S.X. Dou, Phys. Rev. B 65 (2002), 132508.
[26] C. Buzea, T. Yamashita, Supercond. Sci. Technol. 14 (2001) R115.
[27] D.K. Finnemore, J.E. Ostenson, S.L. Bud'ko, G. Lapertot, P.C. Canfield, Phys. Rev. Lett. 86 (2001) 2420.
[28] S.R. Ghorbani, X.L. Wang, M.S.A. Hossain, S.X. Dou, S.-Ik Lee, Supercond. Sci. Technol. 23 (2010), 025019.
[29] S.R. Ghorbani, X.L. Wang, M. Shahbazi, S.X. Dou, C.T. Lin, Appl. Phys. Lett. 100 (2012), 212601.
[30] X.L. Wang, S. Soltanian, M. James, M.J. Qin, J. Horvat, Q.W. Yao, Q.W. Liu, S.X. Dou, Physica C 63 (2004) 408.
[31] X.L. Wang, S.X. Dou, M.S.A. Hossain, Z.X. Cheng, X.Z. Liao, S.R. Ghorbani, Q.W. Yao, J.H. Kim, T. Silver, Phys. Rev. B 81 (2010), 224514.
[32] S.X. Dou, O. Shcherbakova, W.K. Yeoh, J.H. Kim, S. Soltanian, X.L. Wang, C. Senatore, R. Flukiger, M. Dhalle, O. Husnjak, E. Babic, Phys. Rev. Lett. 98 (2007), 097002.
[33] X.L. Wang, S.H. Zhou, M.J. Qin, P.R. Munreo, S. Soltanian, H.K. Liu, S.X. Dou, Physica C 385 (2003) 461.
[34] M. Eisterer, Supercond. Sci. Technol. 20 (2007) R47.
[35] C. Tarantini, H.U. Aebersold, V. Braccini, G. Ferdeghini, V. Ferrando, U. Gambardella, F. Gatti, E. Lehmann, P. Manfrinetti, D. Marré, A. Palenzona, I. Pallecchi, A.S.S.I. Sheikin, M. Putti, Phys. Rev. B 73 (2006), 134518.